Thermal effects and biological response of breast and pancreatic cancer cells undergoing gold nanorod-assisted photothermal therapy

Leonardo Bianchi [a, b, 1], Sara Baroni [b, 1], Gabriela Paroni [b], Martina Bruna Violatto [b], Giulia Yuri Moscatiello [b], Nicolò Panini [c], Luca Russo [b], Fabio Fiordaliso [b], Laura Colombo [b], Luisa Diomede [b], Paola Saccomandi [a, *], Paolo Bigini [b, **]

[a] Department of Mechanical Engineering, Politecnico di Milano, 20156 Milan, Italy
[b] Department of Molecular Biochemistry and Pharmacology, Istituto di Ricerche Farmacologiche Mario Negri IRCCS, 20156 Milan, Italy
[c] Department of Oncology, Istituto di Ricerche Farmacologiche Mario Negri IRCCS, 20156 Milan, Italy

ARTICLE INFO

ABSTRACT

To increase the therapeutic efficacy of nanoparticle (NP)-assisted photothermal therapy (PTT) and allow for a transition toward the clinical setting, it is pivotal to characterize the thermal effect induced in cancer cells and correlate it with the cell biological response, namely cell viability and cell death pathways. This study quantitatively evaluated the effects of gold nanorod (GNR)-assisted near-infrared (NIR) PTT on two different cancer cell lines, the 4T1 triple-negative breast cancer cells and the Pan02 pancreatic cancer cells. The interaction between nanomaterials and biological matrices was investigated in terms of GNR internalization and effect on cell viability at different GNR concentrations. GNR-mediated PTT was executed on both cell lines, at the same treatment settings to allow a straightforward comparison, and real-time monitored through thermographic imaging. A thermal analysis based on various parameters (*i.e.*, maximum absolute temperature, maximum temperature change, temperature variation profile, area under the time-temperature change curve, effective thermal enhancement (ETE), and time constants) was performed to evaluate the treatment thermal outcome. While GNR treatment and NIR laser irradiation alone did not cause cell toxicity in the selected settings, their combination induced a significant reduction of cell viability in both cell lines. At the optimal experimental condition (*i.e.*, 6 μg/mL of GNRs and 4.5 W/cm^2 laser power density), GNR-assisted PTT reduced the cell viability of 4T1 and Pan02 cells by 94% and 87% and it was associated with maximum temperature changes of 25 °C and 29 °C (*i.e.*, ~1.8-fold increase compared to the laser-only condition), maximum absolute temperatures of 55 °C and 54 °C, and ETE values of 78% and 81%, for 4T1 and Pan02 cells, correspondingly. Also, the increase in the GNR concentration led to a decrease in the time constants, denoting faster heating kinetics upon irradiation. Furthermore, the thermal analysis parameters were correlated with the extent of cell death. Twelve hours after NIR exposure, GNR-assisted PTT was found to mainly trigger secondary apoptosis in both cell lines. The proposed study provides relevant insights into the relationship between temperature history and biological responses in the context of PTT. The findings contribute to the development of a universal methodology for evaluating thermal sensitivity upon NP-assisted PTT on different cell types and lay the groundwork for future translational studies.

1. Introduction

Relying on laser exposure, near-infrared (NIR) photothermal therapy (PTT) has been proposed as a therapeutic strategy for tumor treatment [1]. This methodology has demonstrated relevant effectiveness against neoplastic cells, regardless of specific molecular phenotypes [2,3]. Moreover, the minimally invasive nature of the procedure allows for the reduction of operative trauma, shorter treatment duration, and faster recovery times.

Overall, NIR laser-induced hyperthermia and ablation have shown minimal severe adverse effects which are typically associated with conventional cancer therapies [4]. However, the potential risk of either ex-

ceeding the necessary thermal dose, thus leading to undesired healthy tissue damage, or sub-treating the tumor area still poses a concern for the effective application of PTT in the clinical setting [5].

The possibility of generating laser ablations with higher selectivity and better anatomical precision is therefore essential. In photothermal procedures, the efficacy of treatment largely depends on the distribution of temperature within the targeted area and the overall tumor thermal history [6]. One of the most interesting strategies to localize the thermal effect is gold nanoparticle (NP)-assisted PTT, relying on the combined approach between the use of lasers at specific wavelengths [7,8], and the administration of gold NPs in the tumor mass [9–11]. Indeed, it has been demonstrated that nanoscopic bodies having relevant plasmonic properties are capable of generating microenvironment-localized hyperthermia and minimal dispersive diffusion due to the use of gold [12].

Among the different NPs employed in PTT [13–16] gold nanorods (GNRs) have exhibited intriguing characteristics once exposed to NIR laser light [17–21]. Indeed, the electromagnetic field associated with laser light causes the oscillation of the free electrons of the GNRs in the conduction band, and, in these conditions, if the light frequency corresponds to the one of the electron oscillations, the phenomenon of surface plasmon resonance can be observed. The surface electric field increases due to the surface plasmon excitation. An advantageous feature of GNRs is the typically high absorption efficiency, defined as the ratio between the absorption cross-section and the geometric cross-section [22,23].

Moreover, GNRs are characterized by two different surface plasmon absorption bands: the longitudinal oscillation of the electrons of the conduction band makes the long-wavelength band lie in the NIR spectral range, whereas the weak short-wavelength band lies in the visible region of the spectrum due to the transverse oscillation of electrons.

To maximize the photothermal conversion efficiency upon GNR-mediated PTT, the ease of tunability associated with GNRs can be exploited to synthesize GNRs with specific aspect ratios enabling sharp absorbance peak in the NIR region, in correspondence with the wavelength of the therapeutic laser beam.

To enhance the therapeutic outcome of GNR-mediated PTT, real-time temperature monitoring during the procedure represents a pivotal aspect since the temperature history to which the cells are subjected is related to cellular thermal damage [24,25]. Several *in vitro* studies investigated the dose effect of a broad type of NPs on cell viability upon different irradiation conditions [26]. However, a limited number of studies performed a quantitative thermal analysis to correlate the cellular viability with the thermal outcome generated during the NIR irradiation [27], and ultimately assess the thermal sensitivity of cancer cells [28].

Although, in the last decades, many studies have been carried out aimed at identifying specific molecular targets, different tumors are still not responsive to the treatments currently available, such as surgery, radiation therapy, and chemotherapy. To overcome this pharmacokinetic and pharmacodynamic impasse, alternative approaches, such as NP-mediated PTT, are needed and, hence, should be thoroughly characterized.

To this end, in the present study, we aimed to evaluate the *in vitro* efficacy of GNR-assisted PTT on cellular models of neoplasia with poor prognosis, still lacking reliable therapies [29–33]. In particular, we used the triple-negative murine 4T1 cell line as a model of breast cancer lacking pharmacological targets and the murine pancreatic ductal adenocarcinoma Pan02 cells, as a well-established model of pancreas malignancy [34]. We first evaluated the dose- and time-dependent effect of GNRs on cell growth and viability, their internalization, and cellular localization. We then performed GNR-mediated PTT, combined with a thermal analysis based on the maximum temperature, temperature variation profile, the area under the time-temperature change curve, effective thermal enhancement (ETE), and time constants, considering

the step response of a first-order system as a model. The effect of GNR-mediated PTT on the 4T1 and Pan02 viability and cell death pathways was determined and correlated with the results attained from the thermal analysis.

2. Materials and Methods

2.1. GNR Characterization

In the present study, we decided to utilize 11-mercaptoundecyltrimethylammonnium bromide (MUTAB)-coated GNRs as MUTAB was demonstrated to avoid surfactant-related cytotoxicities compared to the other commonly used coatings such as cetyltrimethylammonium bromide which is toxic when dissociated from the GNRs [35,36]. Moreover, MUTAB proved to be a superior coating for the uptake and transport of GNRs by different cell types [37] as compared for instance to polyethylene glycol, which decreases cell uptake [38]. MUTAB-coated GNRs (Nanopartz™, Inc., Loveland, CO, USA) were characterized by different techniques. First, transmission electron microscopy (TEM) was employed to investigate their structure. The stock solution (5 μg/mL of GNRs in water) was vortexed and sonicated. Then, a quantity of 10 μL of the suspension was deposited on a 100-mesh copper electron microscopy grid with formvar coating. After 15 min, the excess was removed with Whatman filter paper, and once the grid was air-dried, Zeiss Libra 120 EFTEM was used for the observation. Images were acquired with an integrated CCD camera equipped with a YAG scintillator. To investigate the dispersion of GNRs, Atomic Force Microscopy (AFM) was employed. AFM evaluations were performed using Multimode AFM with a Nanoscope V system (Veeco/Digital Instruments, Mannheim, Germany). The instrument operated in tapping mode modality. Moreover, the absorption profile in the 400–1000 nm spectral range was acquired by spectrophotometric analysis (Infinite M200, Tecan, Männedorf, Switzerland).

2.2. Cells and Proliferation

4T1 cells (ATCC, CRL-2539) were cultured in RPMI 1640 (GIBCO, 32404–014) supplemented with stable L-Glutamine (Euroclone, ECM2001L), Penicillin (100 UI/mL)/Streptomycin (100 μg/mL) (GIBCO, 15140122) and 10% heat-inactivated fetal bovine serum (FBS, Microtech). Cells were cultured at 37 °C in a humidified 5% CO_2 and routinely split every 3–4 days. PAN02 cells (NIH) were cultured in Advanced RPMI 1640 (GIBCO, 12633–012) supplemented with L-Glutamine (Euroclone, ECM2001L), Penicillin (100 UI/mL)/Streptomycin (100 μg/mL) (GIBCO, 15140122) and 10% heat-inactivated fetal bovine serum (FBS, Microtech). Cells were cultured at 37 °C in a humidified 5% CO_2 and routinely split every 3–4 days.

Different cell concentrations (1–4 × 10^4 cells/well) were tested to evaluate the proliferation. 4T1 and Pan02 cell lines were seeded in 24-well plates, and at the appropriate time points (24, 48, and 72 h), viable cells were counted using the Vi-CELL XR Cell Viability Analyzer (Beckman Coulter).

2.3. GNR Effect on Cell Viability

The possible effect of GNRs on cell viability was evaluated by performing MTT (3-(4,5-dimethylthiazol-2-yl)-2,5-diphenyltetrazolium bromide) assay and counting viable cells.

For the MTT assay, 4T1 and Pan02 cells (2 × 10^4 and 1.5 × 10^4 cells/well, respectively) were seeded in 96-well plates. After 24 h, cells were incubated with GNRs at different concentrations (1.5–120 μg/mL). Control cells were treated with an equivalent volume of the medium. Forty-eight hours post incubation with GNRs, cells were treated for 4 h at 37 °C with MTT compound. Then, the MTT was carefully removed, and the cells were resuspended in acidified isopropanol

(0.04 M HCl). Cell viability was finally determined by measuring the absorbance at 560 nm using a spectrophotometer.

Viable cells were also evaluated using the Vi-CELL XR Cell Viability Analyzer. 4T1 and Pan02 cells (2×10^4 and 1.5×10^4 cells/well, respectively) were seeded in 24-well plates. After 24 h, cells were incubated with GNRs at different concentrations (1.5–120 μg/mL). Control cells were treated with an equivalent volume of the medium. Forty-eight hours post incubation with GNRs, adherent viable cells were collected by trypsinization and counted by Trypan Blue assay.

2.4. GNR Internalization

Confocal and super-resolution microscopy were used to evaluate the GNR internalization into 4T1 and Pan02 cells. Cells were seeded in 24-well plates at a density of 2×10^4 (4T1) or 1.5×10^4 (Pan02) cells/well. The day after, cells were incubated for 24 or 48 h with GNRs at concentrations of 1.5, 3, or 6 μg/mL. The controls were not subjected to any treatment. Cells were washed three times in 10 mM phosphate-buffered saline (PBS), fixed with 4% paraformaldehyde for 40 min, and permeabilized for 1 min with a solution of PBS containing 0.2% Triton X100. Then, a blocking step in PBS - Triton X100 0.2% - bovine serum albumin (BSA) 2% for 30 min was performed before washing with PBS. For microtubule staining, the cells were incubated with the primary antibody alpha-tubulin (1:100, Cell Signaling Tech) diluted in Triton X-100 0.2% - BSA 2% for 2 h at room temperature (RT). After a washing step, a secondary FITC conjugated antibody, Alexa488, (1:1000, Invitrogen) was incubated for 1 h at RT in a PBS - Triton X100 0.2% - BSA 2% solution. At the end of incubation, wells were washed with PBS, and nuclei were stained with Hoechst 33258 (2 μg/mL in PBS, for 10 min). Glass slides were taken from the wells, mounted on cover glass slides with 2–3 drops of Fluoromount, and stored at 4 °C until acquisition. Regarding confocal and super-resolution microscopy, Nikon A1 Confocal and Nikon N-SIM microscopes were employed. The signals associated with Hoechst and Alexa488 were visualized with laser excitation wavelengths at 405 and 488 nm, respectively. Nikon NIS-Element Software was utilized to obtain three-dimensional (3D) rendering and super-resolution reconstructions. Reflectance imaging allowed for the visualization of unlabeled GNRs both for confocal and SIM acquisitions [39].

2.5. GNR-mediated PTT

4T1 and Pan02 were seeded in 24-well plates (2×10^4 and 1.5×10^4 cells/well, respectively). The day after, cells were incubated with GNRs at different concentrations (1.5, 3, and 6 μg/mL). After 24 h from incubation, the culture medium was removed, and a fresh one was added. Contactless laser irradiation was performed with an 808 nm-diode laser (LuOcean Mini 4, Lumics, Berlin, Germany). The beam spot was chosen to cover the entire area of a well (well diameter: 15.6 mm), and the laser power was 9.1 W (power density of around 4.5 W/cm²). The laser operated in a continuous-wave mode, and the exposure time was approximately 300 s for each irradiation. Thermographic imaging was used to real-time monitor the temperature during experiments (FLIR System, T540 with 464×348 pixels spatial resolution, $\pm$ 2 °C accuracy, 10 fps acquisition rate) (Fig. 1). After 24 h from irradiation, viable cells were evaluated using the Vi-CELL XR Cell Viability Analyzer (Beckman Coulter). Experiments were performed in triplicates.

2.6. Apoptosis Assay

4T1 and Pan02 were seeded in 24-well plates at a concentration of 1×10^4 and 1.5×10^4 cells/well, respectively. Twenty-four hours after cell seeding, cells were incubated with GNRs at different concentrations (3 and 6 μg/mL). After 24 h from incubation, the culture medium was replaced with a fresh one, and contactless laser irradiation and temperature monitoring were performed as described in the previous section, '*GNR-mediated PTT.*' After 12 h from laser irradiation, cells were collected and stained with FITC Annexin V Apoptosis Detection Kit with propidium iodide (PI) (BioLegend, #640914), following the manufacturer's instructions. Briefly, cells were collected, centrifuged, washed once in PBS + 5% FBS, and stained with FITC Annexin V in binding buffer for 15 min at RT. For staining of necrotic cells, PI was added before analysis. Cells were analyzed by Flow Cytometer (Cytoflex LX, Beckman Coulter), and the percentage of live, necrotic, early, and late apoptotic cells were calculated by Kaluza analysis software (Beckman Coulter).
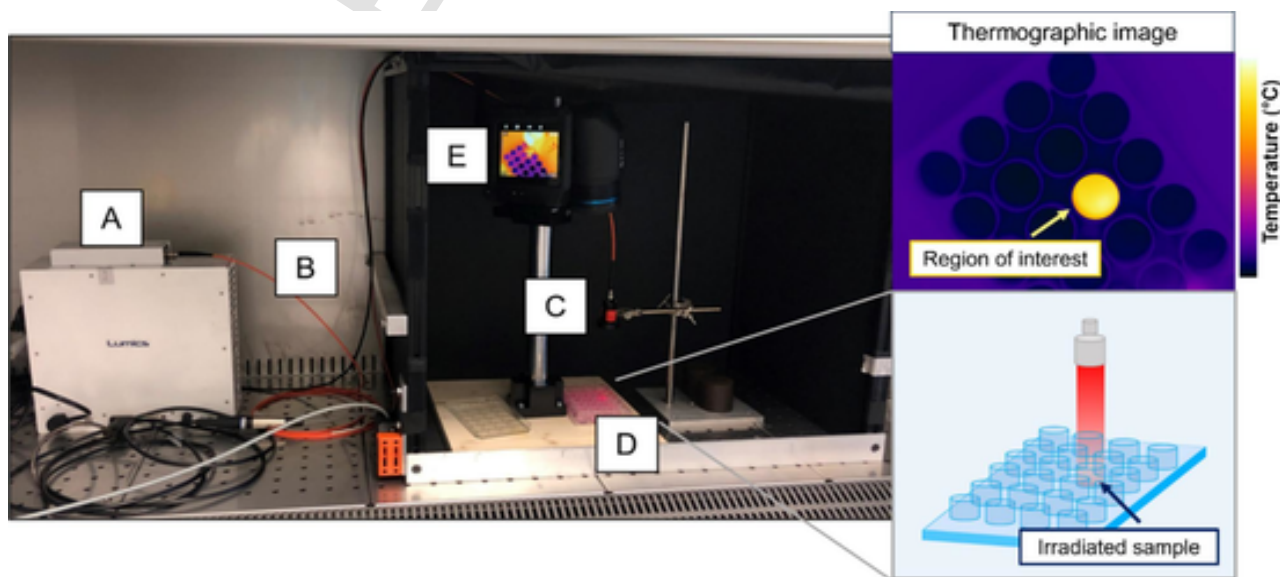

Fig. 1. Picture of the experimental setup used to perform *in vitro* GNRs-mediated PTT experiment. The A) diode laser, B) laser optical fiber, C) laser beam collimator, D) cellular sample, and E) thermographic camera for temperature monitoring. The sketch on the right represents the irradiated sample and the region of interest defined in the thermographic image according to the dimension of the well of 24-well plates, in which cells were seeded.

2.7. Thermal Analysis

The temperature evolution of the samples undergoing NIR irradiation was monitored during the entire photothermal exposure. For each irradiated sample, a region of interest (ROI) was defined in the thermographic image according to the dimension of a well of 24-well plates, in which cells were seeded (Fig. 1). The average value of pixels of the defined ROIs was 1757 ± 316. For each ROI, the average temperature value was calculated considering an emissivity value of 0.95, and the following measurement conditions: relative humidity of 50%, ambient temperature equal to 22 °C, and reflected temperature equal to 22 °C. The performed thermal analysis consisted of the evaluation of the maximum temperature, the temperature change over time, the maximum temperature change, and the area under the temperature change *vs.* exposure time curve.

Furthermore, the temperature trends over time attained through thermographic imaging were used to calculate the time constants (τ) related to the irradiated cancer cells, considering, as a model, the step response of a first-order system. The purpose of this analysis was to quantitatively assess the transient thermal response induced by laser irradiation on 4T1 and Pan02 samples either pre-treated with GNRs or in the absence of GNRs. The response time was estimated by applying linear regression on the natural logarithm of the error fraction function $\Gamma(t)$, described as:

$$\Gamma(t) = \frac{T(t) - T_{ss}}{T_{initial} - T_{ss}} = e^{-\frac{t}{\tau}} \tag{1}$$

being $T(t)$ the temperature value at the instant of time t, $T_{initial}$ the initial temperature at the beginning of the step, and T_{ss} the estimated temperature value at the steady state. Besides, the percentage of the ETE was calculated as the difference between the average values of maximum temperature change attained during GNR-mediated PTT at a specific concentration i (1.5, 3, or 6 μg/mL) and the maximum temperature change obtained during laser irradiation experiments without GNRs assistance, divided by the average value of the maximum temperature change obtained during laser irradiation experiments without GNRs assistance:

$$\text{ETE } (\%) = \frac{\text{maximum temperature change}_{GNRs,i+Laser} - \text{maximum temper}}{\text{maximum temperature change}_{Laser}}$$

2.8. Statistical Analysis

Data are analyzed using GraphPad Prism Software (version 9.0). Data are presented as mean ± SD. One-way or two-way ANOVA test and Bonferroni's *post hoc* test were used for the comparison of multiple groups. Differences with *p* values <0.05 were considered statistically significant.

3. Results

3.1. GNR Characterization

Before proceeding with biological studies, GNRs were characterized to assess their main physicochemical parameters, such as size, shape, and absorption profile. According to TEM image analysis (Fig. 2A), the GNRs showed an elongated rod-shaped morphology with a diameter of 10.3 ± 1.0 nm and a length of 44.0 ± 4.3 nm, hence an aspect ratio of around 4.3. Fig. 2B shows representative images of GNRs at two different magnifications. They are monodisperse with a cylindrical shape peculiar to rod-shaped NPs without forming large aggregates in the system. Finally, the absorption spectrum revealed a peak absorption at 808 nm (Fig. 2C).

3.2. Effect of GNRs on Cell Viability

Following the characterization analyses that confirmed the stability of GNRs and before testing their cytotoxic effect, we evaluated the cellular growth over time. Different cell concentrations (1–4 × 10⁴ 4T1 cells/well and 1–2 × 10⁴ Pan02 cells/well) were seeded on 24-well-plates. The proliferation was monitored by counting the viable cells at increased time points (Supplementary Fig. S1). Based on the data collected, we decided to seed 2 × 10⁴ 4T1 cells/well and 1.5 × 10⁴ Pan02 cells/well in the subsequent assays.

Cell viability experiments were performed to select GNR concentrations that did not affect the cell viability after 48 h from the treatment. To this end, 4T1 and Pan02 cells were incubated with 1.5–120 μg/mL GNRs. As shown in Fig. 3, regarding both 4T1 and Pan02 cell lines, a significant difference with control was observed starting from 12 μg/mL GNRs. Indeed, a dose-dependent effect was measured independently from the type of cell line. The concentrations of 1.5, 3, and 6 μg/mL GNRs did not affect the cell viability. Hence, they were all chosen for the subsequent GNR-mediated PTT experiments in order to carry out a more comprehensive characterization of the thermal effect induced by photothermal treatment in the two cellular lines.

3.3. GNR Internalization

The ability of GNRs to be internalized by 4T1 and Pan02 cells was evaluated by confocal and super-resolution microscopy. Fig. 4 shows the localization of GNRs in 4T1 and Pan02 cells. The red signal is associated with GNRs, while cells are identified by the presence of nuclei in blue and cytoskeleton in green (tubulin staining). The confocal analysis
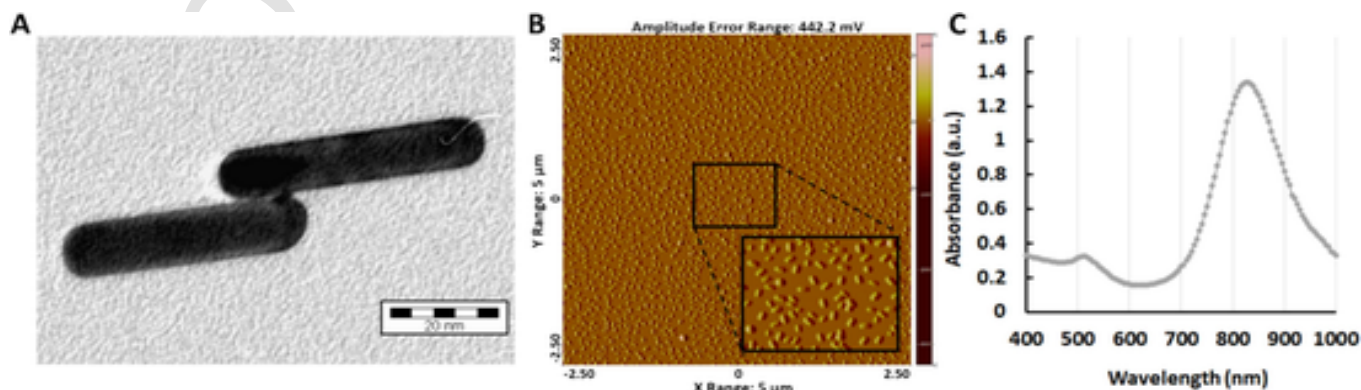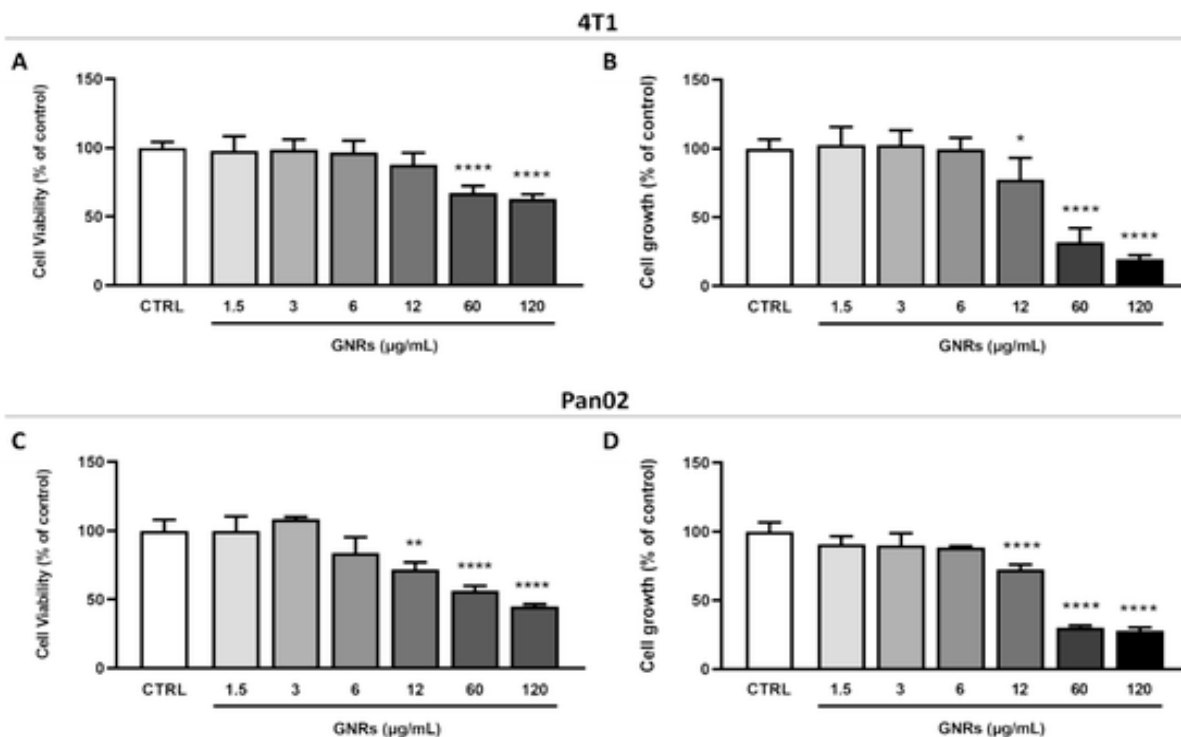

Fig. 2. GNR characterization. A) Transmission Electron Microscopy, B) Atomic Force Microscopy, C) absorbance spectrum of the GNR stock solution.

Fig. 3. Effect of GNRs on cell viability (MTT assay) and growth (number of viable cells expressed as a percentage of the control). A, B) 4T1 and C, D) Pan02 cells were treated with 1.5–120 μg/mL or with the same volume of medium (CTRL). A, C) Cell viability and B, D) growth were recorded 48 h after treatment with GNRs. Data are expressed as values normalized on the mean of CTRL cells of 3 independent experiments. *$p < 0.05$, **$p < 0.005$ and ****$p < 0.0001$ *vs.* CTRL according to Ordinary one-way ANOVA.

revealed the presence of the GNRs in the perinuclear zone at 24 and 48 h after the incubation for all the tested concentrations (Fig. 4A and C). The spotted red signal showed that GNRs are confined and presumably clustered into endocytic vesicles, commonly known to mediate cellular internalization and NP processing. A fast and dose-dependent accumulation can be seen in both cell lines. The super-resolution reconstructions observed the internalization of GNRs at 24 h after the incubation (Fig. 4B and D, upper rows). Moreover, the 3D localization of GNRs around single cells confirms the GNRs uptake in both 4T1 and Pan02 cell lines (Fig. 4B and D, bottom rows). The time point of 24 h GNRs-incubation was, hence, chosen for the performance of NIR irradiation to exert GNR-mediated photothermal conversion.

### 3.4. GNR-mediated Photothermal Experiment

The temperature evolution during treatment was monitored through thermographic imaging. The exemplificative thermal images for the different experimental conditions, the temperature change over time of irradiated 4T1 and Pan02 cells either pre-treated with GNRs (1.5, 3, and 6 μg/mL) or not treated with GNRs are shown in Fig. 5, alongside the registered maximum temperature change and the area under the curve.

The association of laser irradiation with pre-treatment with GNRs entailed higher temperature changes compared to laser irradiation alone (Fig. 5C and F). Concerning the 4T1 cell line, the average value of the maximum temperature change in the case of laser irradiation without GNRs was 14 °C. The combination of laser irradiation and GNRs resulted, for all GNR concentrations considered, in a statistically significant increase compared to the laser-only treatment, in terms of maximum temperature change (Fig. 5D). Indeed, the average values of the maximum temperature change were 19 °C, 22 °C and 25 °C for 1.5, 3, and 6 μg/mL GNRs, respectively. Likewise, a statistically significant difference was found between the average value of the area under the curve calculated for laser irradiation without GNRs assistance (*i.e.*, 23029 °C·s) and the value of the areas under the curve of the temperature change *vs.* time calculated for the different laser + GNRs combinations (31981 °C·s, 37407 °C·s and 43153 °C·s, for 1.5, 3 and 6 μg/mL GNRs, respectively (Fig. 5E)).

Regarding the photothermal treatments performed on Pan02 cells, as observed for 4T1 cells, the samples undergoing laser irradiation without GNRs experienced lower temperature change throughout the NIR irradiation (Fig. 5F). In the case of the Pan02 cell line, the average values of the maximum temperature change, registered at the end of the laser irradiation, were 16 °C, 20 °C, 25 °C and 29 °C, for the conditions of the laser without GNRs, laser + 1.5 μg/mL GNRs, laser + 3 μg/mL GNRs, and laser + 6 μg/mL GNRs, accordingly (Fig. 5G). Moreover, the average values of the area under curve of the temperature change as a function of time were 26969 °C·s in the case of laser irradiation in the absence of GNRs, and 35976 °C·s, 43826 °C·s and 52468 °C·s for the laser irradiation combined with GNR assistance, respectively for 1.5, 3 and 6 μg/mL GNR concentrations (Fig. 5H). Statistically significant differences were observed between the samples subjected to laser irradiation without GNRs and the different laser + GNRs combinations for both the maximum temperature change (Fig. 5G) and the area under the curve (Fig. 5H). According to the presented results, the combination of 6 μg/mL GNR pre-treatment and laser irradiation led to a ~ 1.8-fold increase in the average maximum temperature change for both 4T1 and Pan02, compared to the laser-only condition. Table 1 also reports the maximum temperature, the time constants, and the ETE related to the different photothermal experiments performed on 4T1 and Pan02 cell lines.

For both cell lines, the maximum absolute temperature registered for the NIR laser treatment in the absence of GNRs was equal to 40 °C. By increasing the concentration of GNRs, a consequent rise in the maxi-
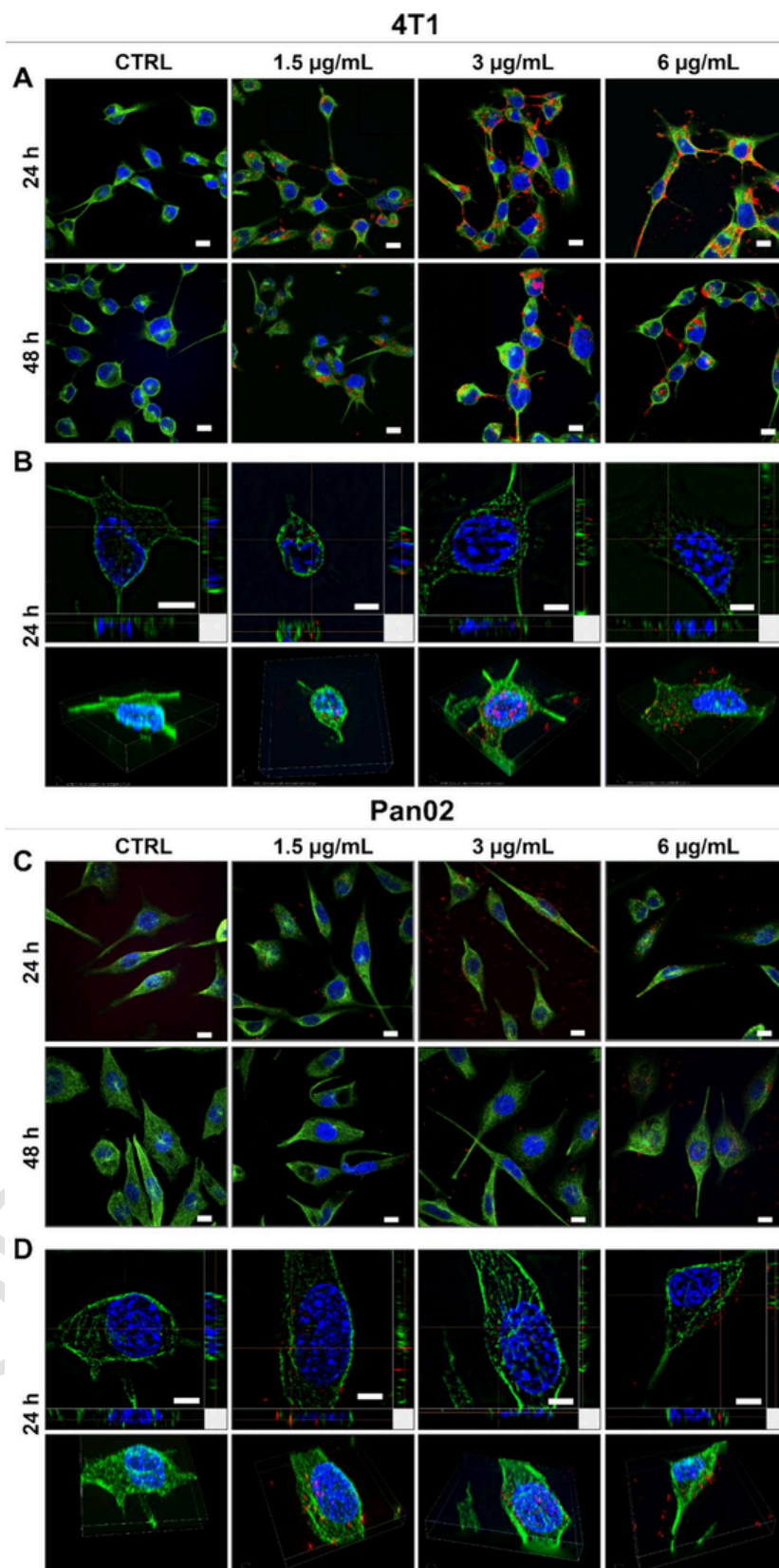
Fig. 4. GNR internalization. Representative images of GNR-cell interaction. GNR agglomerates are depicted in red, tubulin in green, and nuclei in blue. 4T1 cells: A) confocal images collected at 24 and 48 h from the incubation with different concentrations of GNRs (1.5–6 μg/mL). Scale bar, 10 μm. B) Super-resolution recon-

Fig. 4.—*continued*

structions by the orthogonal projection of the three-dimensional stack of single cells (upper row) and corresponding 3D rendering (bottom row). Scale bar, 5 μm. Pan02 cells: C) confocal images at 24 and 48 h from the incubation with different concentrations of GNRs (1.5–6 μg/mL). Scale bar, 10 μm. D) Super-resolution reconstructions by the orthogonal projection of the 3D stack of single cells (upper row) and corresponding 3D rendering (bottom row). Scale bar, 5 μm. (For interpretation of the references to colour in this figure legend, the reader is referred to the web version of this article.)
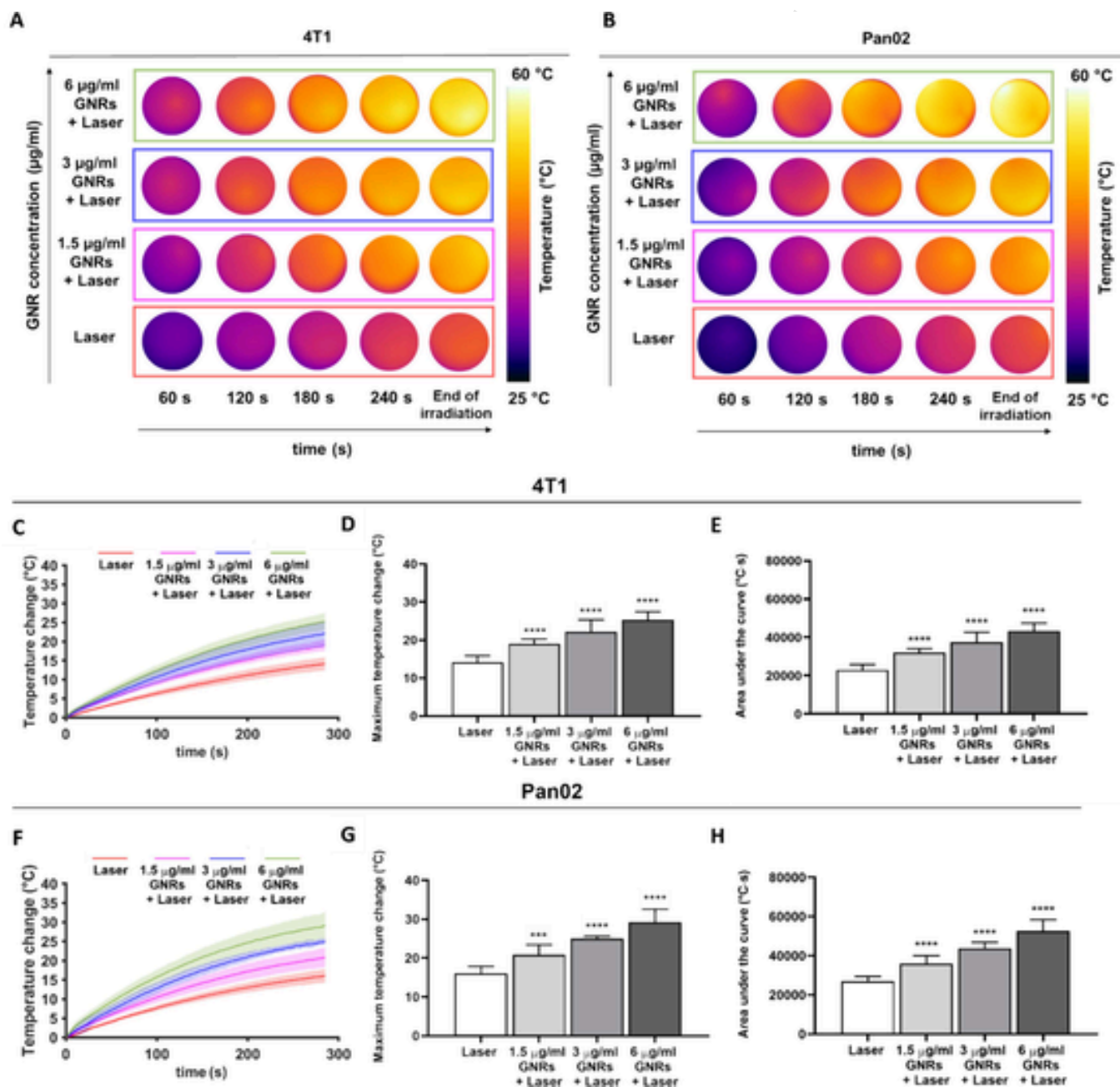

Fig. 5. Exemplificative thermal images of the samples exposed to laser irradiation. Cells were either exposed to laser irradiation (Laser) or pre-treated with 1.5, 3, or 6 μg/mL of GNRs and exposed to laser (GNRs + Laser), thermographic imaging was employed to monitor the temperature evolution during photothermal treatments, as described in the Materials and methods section. The thermal maps show the temperature distribution, within the ROIs defined for the thermal analysis, at different instants of time of the photothermal exposures: A) 4T1 and B) Pan02 cancer cells. Thermal analysis concerning GNRs-assisted PTT in 4T1 and Pan02 cells: C) Temperature change over time, D) Maximum temperature change, and E) Area under the curve estimated for the experiments on 4T1 cells. F) Temperature change over time, G) Maximum temperature change, and H) Area under the curve regarding photothermal treatments on Pan02 cells. The mean trends of the temperature change and the SD (shadowed lines) are shown in C and F. In D, E, G, and H, each value is the mean ± SD (N = 4–13), ****p < 0.0001, ***p < 0.0005 relative to Laser, according to Ordinary one-way ANOVA and Bonferroni's *post hoc* test.

Table 1

Values of maximum temperatures (expressed as average value ± SD), time constants (average value ± SD), and the effective thermal enhancements (ETE) attained for the different photothermal experiments performed on 4T1 and Pan02 cell lines.

	Laser	1.5 µg/mL GNRs + Laser	3 µg/mL GNRs + Laser	6 µg/mL GNRs + Laser
4T1				
Maximum temperature (°C)	40 ± 2	43 ± 4	48 ± 5	55 ± 1
Time constant (s)	363.4 ± 68.4	265.7 ± 54.9	264.4 ± 54.9	245.0 ± 54.9
ETE (%)		34	56	78
Pan02				
Maximum temperature (°C)	40 ± 2	44 ± 3	50 ± 1	54 ± 3
Time constant (s)	276.6 ± 62.9	235.4 ± 66.3	228.9 ± 82.8	181.5 ± 33.9
ETE (%)		30	55	81

mum temperature can be observed, up to values of 54–55 °C, attained at the concentration of 6 µg/mL GNRs. Conversely, incrementing the GNR concentration led to an overall decrease of the calculated time constants, denoting faster heating kinetics upon irradiation (*e.g.*, the estimated average values of the time constants were 277–363 s in the case of laser irradiation without GNRs, whereas 6 µg/mL GNRs + laser irradiation, the time constants were 182–245 s. Finally, the calculated values of the ETE (Table 1) are similar for both cell lines at the different GNR concentrations and show a proportional increase with GNR concentration. At the lowest GNR concentration (1.5 µg/mL GNRs), ETE equal to 34% and 30% were registered for 4T1 and Pan02, correspondingly; at 3 µg/mL GNRs, ETE for 4T1 and Pan02 was 55% and 56%, whereas, the highest concentration considered, 6 µg/mL GNRs, was associated with the maximum enhancement, *i.e.*, ETE was 78% and 81%, for 4T1 and Pan02, accordingly.

The results concerning the viability of the cells undergoing GNR-mediated PTT are depicted in Fig. 6A and C for 4T1 and Pan02 cancer cells, respectively (each value is the mean ± SD, *N* = 4–13). Representative bright-field microscopy images of cells subjected to GNR-mediated PTT are reported in Fig. 6B and D, for 4T1 and Pan02 cancer cells, accordingly.

In the histograms reported in Fig. 6A and C, the cells subjected only to pre-treatment with GNRs were shown to be comparable with controls (cells neither treated with GNRs nor NIR irradiated) in terms of cell viability, as no statistically significant differences were found. Similar data were found for cells subjected only to NIR laser irradiation. Conversely, in both the cell types, the combination of NIR laser irradiation and GNRs induced a statistically significant decrease in cell viability proportional to the GNR concentrations tested. Concerning the experiment on 4T1 cells, the average values of cell growth (% of control) for the cells pre-treated respectively with 1.5, 3, and 6 µg/mL of GNRs and undergoing laser irradiation were 40%, 21%, and 6%, after 24 h from irradiation. Regarding Pan02 cells, average values in terms of cell growth (% of control) were 63%, 14%, and 13%, for the cells pre-treated with 1.5, 3, and 6 µg/mL of GNRs, accordingly, and subjected to laser exposure. In addition, the combination of GNRs and NIR laser irradiation modified the cellular morphology of 4T1 and Pan02 cells which appeared less bright, more roundly shaped, and detached from the growth surface, compared to the other conditions tested (Fig. 6B and D).

To decipher the nature of the loss of viable cells after treatment of the cell lines with the combination of GNRs and NIR laser irradiation, we first executed anew GNR-mediated PTT experiments with the same laser settings and at the most effective GNR concentrations (*i.e.*, 3 and 6 µg/mL) in terms of reduction of cell viability (Fig. 6) and then performed Annexin V/Propidium Iodide (PI) Apoptosis Assay. The assay allows to monitor the presence of necrotic and apoptotic cells. In particular, it is possible to distinguish between early (characterized by the

translocation of phosphatidylserine to the outer leaflet of the lipid bilayer) and late apoptosis or secondary necrosis (characterized by phosphatidylserine externalization and permeabilization of the cell membrane allowing the entry of dyes such as PI) [40]. The results of the thermal analysis concerning these experiments confirm our previous observations (Fig. 5 and Table 1) and are reported in Supplementary Fig. S2 and Supplementary Table 1. As shown in Fig. 7 (upper panel), only in the case of combined treatment there is an increase in total apoptotic cells (right bottom and upper region of the depicted plots). Indeed, the graph depicts representative flow cytometry dot plots of cells for Annexin V-PI counterstain. X and Y axes represent green and red fluorescence channels corresponding to Annexin V and PI staining respectively. Each plot shows cells positive for Annexin V only (right bottom region, RB), positive for PI only (left upper region, LU), positive for both (right upper region, RU), and negative for both (left bottom region, LB). Regions RB, LU, RU and LB represent early apoptotic, necrotic, late apoptotic and live cells in the population. In detail, at the observed time frame post-treatment (12 h after laser irradiation), there is mainly an increase in late apoptosis. Late apoptotic cells represent 30% and 40% of all the cells treated with 3 µg/mL and 6 µg/mL GNRs plus NIR laser irradiation. Early apoptosis is observed only at the higher concentration of GNRs administered (6 µg/mL) when the total apoptosis is massive (54.12%) and consists of 13.5% of the total cell population. Interestingly in the case of a classical apoptotic compound, such as VP-16 (etoposide), a small effect on cell viability (viable cells decrease of about 20%) was associated with 17% of total apoptotic cells with a higher percentage of early apoptosis (6.2%) and a lower percentage of late apoptosis (11.2%) compared to the combo of GNRs and NIR laser irradiation (Supplementary Fig. S3). In the case of Pan02 (lower panel) again late apoptotic cells represent the majority of dead cells due to the combination of GNRs and NIR laser irradiation treatment. In the context of this cell line, VP-16, which is a well-known apoptosis inducer, generates dead cells in the late apoptotic phase at the time frame considered (47%) with negligible evidence of early apoptotic cells (2%) (Supplementary Fig. S3). This could be due to an intrinsic property of the cell line or to the fact that the chosen time frame is too long to detect early apoptotic events. It should be noted that in this cell line, FACS analysis reveals the presence of a small proportion of necrotic cells (from 12% to 17%) in the case of treatment with GNRs alone (3 µg/mL and 6 µg/mL) that was not detectable by viable cell counting and MTT assay (Fig. 3). It could be that GNR treatment induces the permeabilization of PI during the FACS procedures in a small proportion of cells that are still viable and attached as assessed by the ViCell Coulter Counter analysis and metabolic active (MTT). Altogether the above data suggest that at time frames in which treatment of the cell lines with a single agent does not induce cell death, the combo GNRs plus NIR laser irradiation triggers mainly late apoptosis.

4. Discussion and Conclusions

The present study represents a prodromal step for the characterization of the different parameters that play a role in NP-assisted photothermal stimulation when applied to the biomedical context. We employed two cellular models, prototypes of cancer diseases with poor clinical outcomes: the 4T1 breast cancer cell line [3] and the Pan02 pancreatic adenocarcinoma cell line [34]. Indeed triple-negative breast cancer and pancreatic cancer share common severe progression, high lethality, and scarce therapeutical options with conventional chemotherapy or other alternative pharmacological approaches [41,42].

A particular focus has been reserved on the quantitative evaluation of the thermal effect of GNR-mediated PTT on cells, and its correlation with the biological response. Indeed, considering the final aim to improve PTT efficiency, real-time temperature monitoring during the procedure represents a crucial aspect since the temperature history to
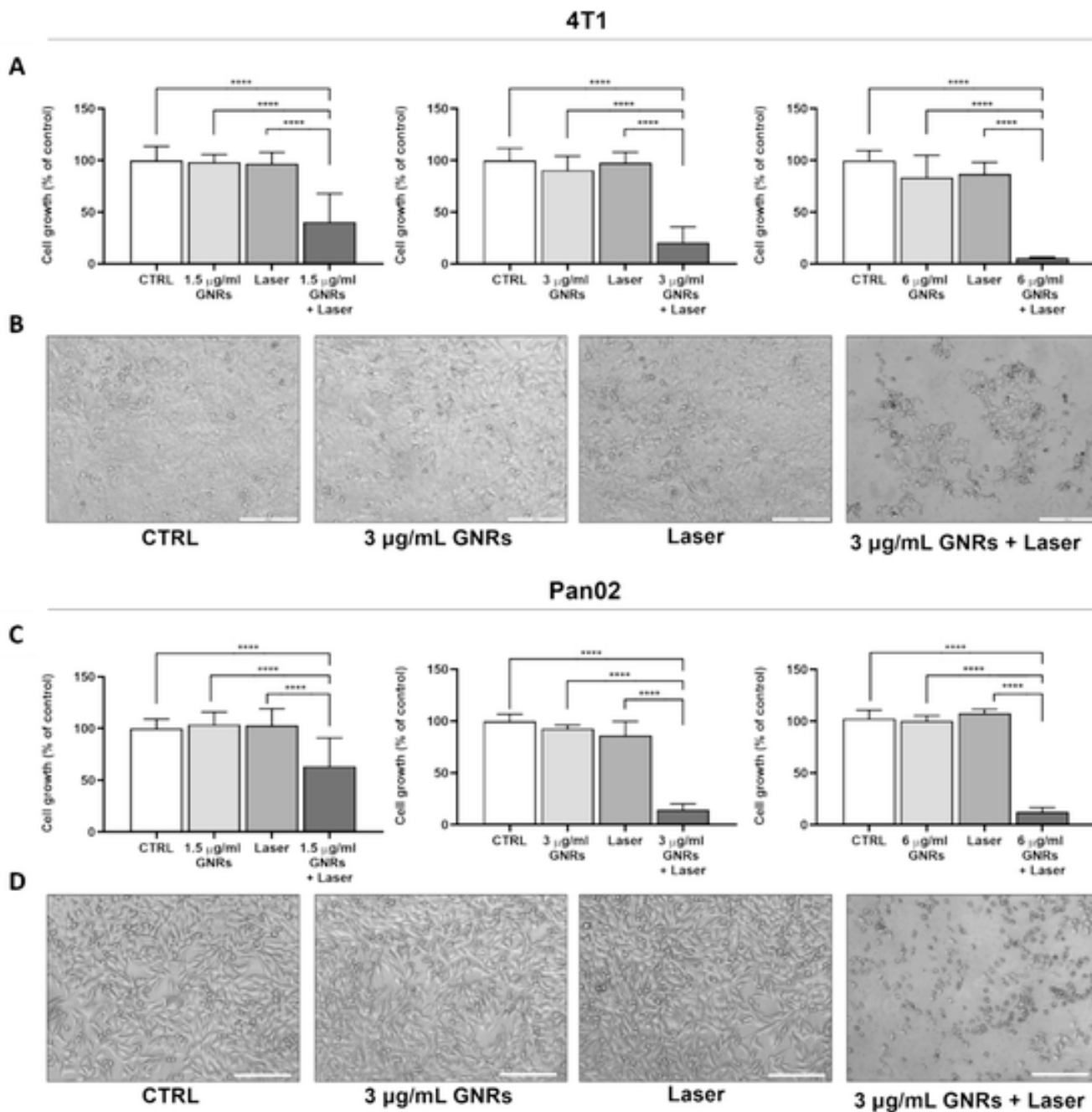
Fig. 6. GNRs-mediated PTT in 4T1 (A and B) and Pan02 cells (C and D). A) Cell growth histograms of 4T1 cells (number of viable cells expressed as a percentage of the control). From left to right plot, cells were treated with 1.5, 3 or 6 μg/mL of GNRs (GNRs), exposed to laser irradiation (Laser) or treated with GNRs and exposed to laser (GNRs + Laser) as described in the Materials and Methods section. Control cells were treated with medium alone (CTRL). Each value is the mean ± SD. ****$p < 0.0001$, two-way ANOVA and Bonferroni's *post hoc* test. Interaction: GNRs (all concentrations)/Laser <0.0001 ****. B) Representative bright-field microscopy images of 4T1 cells treated with 3 μg/mL GNRs, Laser, and 3 μg/mL GNRs + Laser. The white scale bars correspond to 200 μm. C) Cell growth histograms of Pan02 cells. From left to right plot, cells were treated with 1.5, 3 or 6 μg/mL of GNRs (GNRs), exposed to laser irradiation (Laser) or treated with GNRs and exposed to laser (GNRs + Laser). Control cells were treated with medium alone (CTRL). Each value is the mean ± SD. ****p < 0.0001, two-way ANOVA and Bonferroni's *post hoc* test. Interaction: GNRs (all concentrations)/Laser <0.0001 ****. D) Representative bright-field microscopy images of Pan02 cells treated with 3 μg/mL GNRs, Laser, and 3 μg/mL GNRs + Laser. The white scale bars correspond to 200 μm.

which the cells are subjected is related to the tumor thermal damage [10,43]. Indeed, being the temperature the main physiological quantity which triggers a specific biological response, our study has focused on the investigation of the optimal measurement conditions and data processing methods to obtain accurate temperature measurement and useful indices, like the time constant and the ETE [10,44]. This step is aimed also at providing a reliable monitoring system that can be ap-

plied to more complex *in vivo* studies. While in *in vitro* settings most experimental conditions are satisfactorily controlled, in the *in vivo* scenario the biological variability is much larger. Thus, it is crucial to have a preliminary *in vitro* phase in which the technical parameters (*e.g.*, settings of the delivery system, temperature measurement system, and methods for obtaining temperature-related indices) are well character-
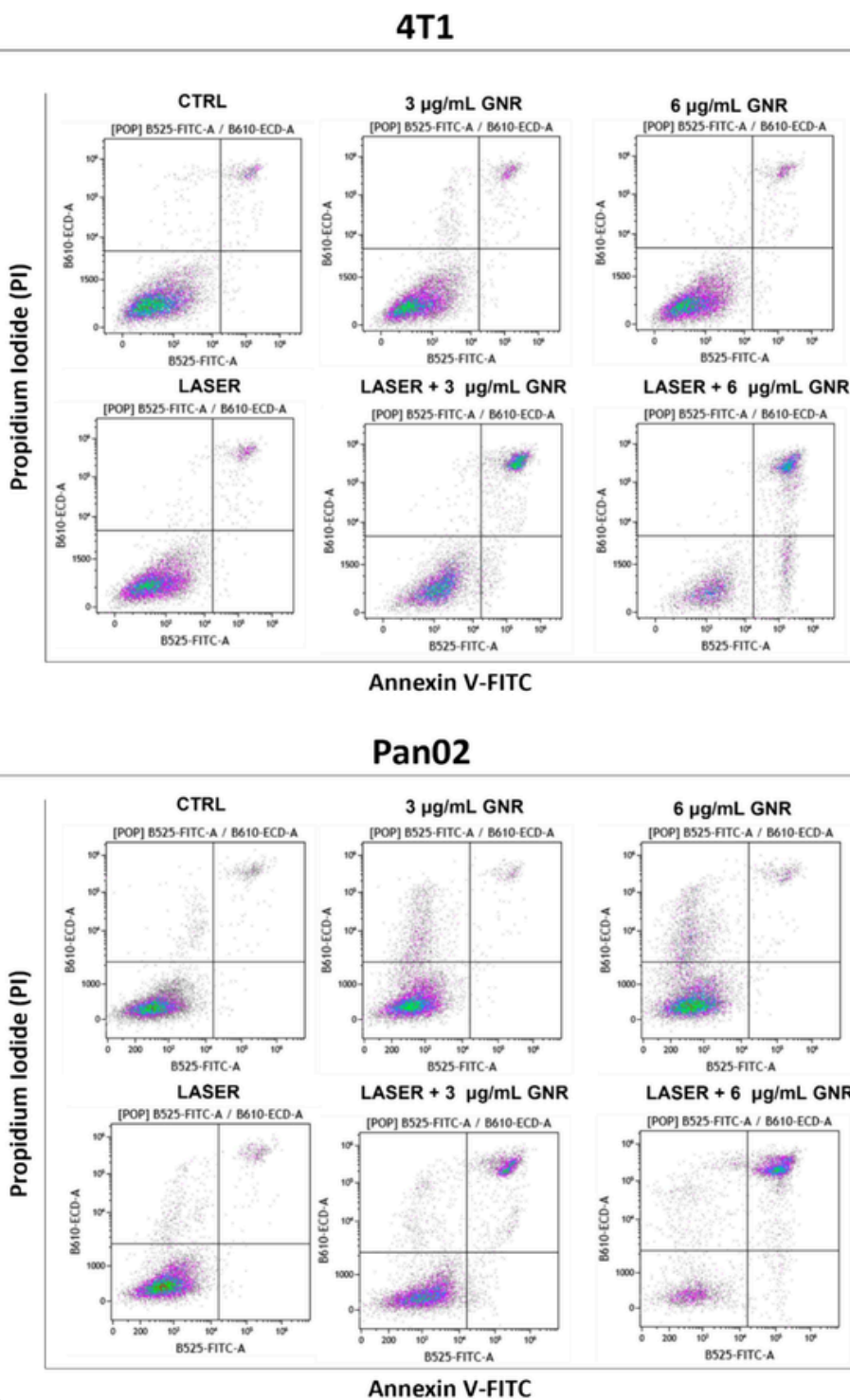
Fig. 7. Analysis of cell death induced by GNRs and PTT treatment. Early apoptosis, late apoptosis, and necrosis were evaluated by flow cytometry after staining with Annexin V-FITC/propidium iodide (PI). Representative dot plots of PI (y-axis) *vs.* Annexin V (x-axis) for 4T1 (upper panel) and Pan02 cancer cells (lower panel).

ized, in order to decrease their effect on the final accuracy of the experimental model.

Several studies have evaluated the therapeutic efficacy of NP-mediated PTT in *in vitro* and *in vivo* scenarios [20,45]. The majority of the experimental reports *in vitro* have focused on the analysis of the cell viability and/or assessment of cell death pathways under different irradiation conditions or NP concentrations on different cancer cell types [20,46]. For instance, Pattani et al. investigated the cell death pathway

response during GNR-assisted PTT, performed at different laser fluence rates, on colorectal tumor cells (HCT-116) [44]. In a recent study, Domingo-Diez et al. performed GNR-mediated PTT with GNRs of two distinct dimensions on murine glioma (CT2A) and murine melanoma (B16F10) cells and evaluated the efficacy of the treatment in terms of cell viability and the type of triggered cell death by dehydrogenase activity, and calcein propidium iodide and Annexin V staining [46]. Moreover, Zhang and colleagues evaluated the temperature-dependent

cell death pathways in murine melanoma cells (B16-BL6) undergoing functionalized GNR-mediated PTT and detected the temperature with an infrared radiation thermometer by moving the laser beam away for a few seconds and then repositioning it back again after the measurement acquisition. They then correlated the final temperature reached during the irradiation with the cell death pattern [27].

Nevertheless, the number of studies that have performed a quantitative thermal analysis to correlate the biological response of the cells with the temperature evolution [47], thus the thermal dose delivered during the NIR irradiation [48], needs to be urgently increased.

Considering the differences in terms of NIR laser irradiation modalities and settings, NP types, and concentrations utilized in PTT, there exists the need to use a common outcome such as the time-temperature data to allow a comparison of different studies on different cell types and a correlation with the biological response upon PTT. In this concern, Happonen et al. employed the thermal isoeffect dose (TID) based on the Cumulative Equivalent Minutes at 43 °C to evaluate the outcome of NP-induced PTT [48]. They performed black porous silicon NP-mediated PTT on HeLa cancer cells and utilized an infrared sensor to real-time monitor and control the temperature of the samples. The TID was originally developed to establish a connection between specific biological endpoints and tissue thermal exposure, maintained for various durations [49–51]. TID is typically employed for thermal treatments characterized by longer exposure times and lower temperatures. Indeed, it has been validated with *in vitro* experiments, focusing on cell survival as the target endpoint, successfully estimating cell death within the temperature range of 40 to 47 °C, which is the thermal interval for which this model was initially devised [49,52–55]. However, higher temperatures (*i.e.*, > 50 °C) can be reached during thermal ablation procedures and NP-assisted PTT [56,57].

Hence, in the present study, we performed *in vitro* GNR-assisted PTT on 4T1 and Pan02 cancer cells at different GNR concentrations and real-time monitored the temperature evolution through thermographic imaging. We firstly evaluated the GNR internalization and effect on cell viability, performed GNR-mediated PTT, and then devised a thermal analysis based on multiple thermal parameters. The cell viability and cell death pathways were explored and correlated with the results of the thermal analysis to propose a universal methodology to evaluate the effect of PTT on different cell types.

We first investigated the interaction between the two cell lines and the gold NPs. It is widely known that the NP geometry can greatly influence their interaction with cells and tissues [58,59] and there is also a large body of evidence demonstrating the potential application of gold NPs with different shapes in PTT [60,61]. In the present work, we decided to select a single type of gold NPs, the rod-shaped (GNRs), for different reasons: to avoid another source of variability dependent on the NP shape [10] and to reach high efficiency in terms of plasmonic resonance. After a relatively long-term exposure (*i.e.*, 48 h), both cell populations well-tolerated concentrations of up to 6 μg/mL of GNRs. Quite interestingly, Pan02 cells showed an increased vulnerability compared to 4T1 cells in terms of cell viability (Figs. 3A and B). Since a clear relationship between the amount of gold NPs internalized in cells and the cytotoxic effect has been widely reported [62,63], we hypothesized that Pan02 had a more efficient uptake. Our confocal analyses seemed to confute this suggestion. The reason why an effect on cell viability occurred at a GNR concentration lower in Pan02 compared to 4T1 may be correlated to a series of downstream events, activated by the interaction with the nanomaterial. While the treatment of 4T1 and Pan02 cells with GNR concentrations up to 6 μg/mL did not induce a cytotoxic effect compared to controls, the combination of GNRs and laser exposure, induced a dramatic toxicity, for all the examined concentrations (1.5, 3, 6 μg/mL), in both cell populations.

In 4T1 cells, the association with NIR laser irradiation allowed reaching the IC50 at a GNR concentration 40 times lower than without laser stimulation (*i.e.*, 1.5 μg/mL, Fig. 6, *vs.* ∼60 μg/mL, Fig. 3). More-over, we found that laser irradiation alone was not able to increase cell toxicity, whereas already at the lowest concentration tested, the combination of laser-GNRs was very effective. Despite some small dissimilarities in quantitative terms, it is worth observing that this phenomenon developed similarly in both cell populations. The cytotoxic effect under NIR exposure was proportional to the GNR concentration. At the highest concentration, the average values of cell growth (% of control) were 6% and 13% for 4T1 and Pan02 cells, respectively, 24 h after the GNR-mediated photothermal exposure. This cytotoxic effect was associated with maximum temperature changes of 25 °C and 29 °C (*i.e.*, ∼1.8-fold increase compared to the laser-only condition), maximum absolute temperatures of 55 °C and 54 °C, areas under the temperature change over time curve of 43153 °C·s and 52468 °C·s, and ETE values of 78% and 81%, for 4T1 and Pan02 cells, accordingly. As observed, at the employed power density, NIR laser irradiation was not able to induce a cytotoxic effect on cells, displaying no statistically significant differences with controls in terms of cell growth (% of control) and cell morphology after treatment. In this case, the corresponding thermal analysis outlined maximum temperature changes of 14 °C and 16 °C, areas under the temperature change over time curve of 23029 °C·s and 26969 °C·s, for 4T1 and Pan02 cells, respectively, and maximum absolute temperatures of 40 °C, for both cell types. Besides, the analysis of the time response indicated a reduction of the time constants due to the presence of GNR upon irradiation, thus showing faster heating kinetics compared to laser irradiation without GNRs, as also observed in previous literature studies *in vivo* conditions [57], and a decrease of time constant proportional to the GNR concentration. Considering the attained results, it is possible to suppose that the increase of laser power may lead to reaching the same temperature achieved by the combined GNR-laser irradiation application and consequent cytotoxicity. However, the present study has been designed to pave the way for translational study. For this reason, the possibility of generating an anatomically selected GNR-mediated hyperthermia will be crucial to realize the best therapeutical index, by the limitation of undesired heating propagation in tissues close to the tumoral mass.

Our study also aimed to start investigating the mechanisms associated with cell death upon GNR-assisted PTT at the most effective GNR concentrations (*i.e.*, 3 and 6 μg/mL). Our results revealed that, while both pre-treatment with GNRs and laser irradiation did not lead to cell death by themselves, their combination induced a significant impairment of cell viability mainly due to late apoptosis or secondary necrosis. Apoptosis indeed is an asynchronous cell death program that is actively engaged by a damaged cell, occurs rapidly, and ends with cell membrane permeabilization leading to the so-called secondary necrosis [40,64]. Even if a time-course analysis would provide a more detailed picture of the timing of the apoptotic process, it is interesting to observe that two inactive stimuli are able to engage a significant cell death program when combined. Interestingly, the two cell lines analyzed in the present study exhibit intrinsic differences in their susceptibility to cytotoxic insults showing variations in VP-16-driven cytotoxicity, a well-established apoptotic and cytotoxic agent (Supplementary Fig. S3). When treated with the same concentration of VP-16 the 4T1 cell line shows a population of both early and late apoptosis. In contrast, the Pan02 cell line displays only late apoptosis at the analyzed time frame. Accordingly, also in the case of the combination of laser + GNRs the mechanism behind the observed cytotoxicity reflects the intrinsic diverse susceptibility of the two cell lines. In the 4T1 cell line, comparable levels of the compound induce early and late apoptosis while the Pan02 cell line develops mainly late apoptosis (Fig. 7). Nevertheless, the main response in the case of the combinatorial treatment laser + GNRs results in a huge secondary necrosis induction. These results are of worth since both the analyzed cell models represent "cold" tumors with a low response rate to emerging cutting-edge immune checkpoint inhibitor (ICI) therapies. The induction of local cytotoxic effects leading to secondary apoptosis and cell breakdown could represent a source of im-

mune stimulation that may help render triple-negative breast cancer and pancreatic cancer more responsive to ICI [65,66].

Our research fits well in the wider scenario of works that aim to initially set up the optimal conditions for an efficient photothermal approach [67–70]. Although a straightforward comparison among the studies is complex due to the different heating modalities, our results are in general agreement with previous investigations elucidating the effect of different temperatures on breast and pancreatic cancer cells. Regarding breast cancer cells, Lee and colleagues observed that when human breast cancer cells (*i.e.*, MCF-7 and MDA-MB-231) were subjected to hyperthermal treatment at or below 47 °C for 45 min, they displayed tolerance. However, elevating the temperature to 52 °C resulted in hyperthermal stress that led to cell death at a rate > 95% [71]. Concerning pancreatic cancer cell lines, Chamani et al. measured the cell viability in Pan02 and KPC cells in the thermal range of 42.5–50 °C for different durations (*i.e.*, 3–60 min) [28]. In accordance with our observations, the higher the temperature, the quicker the rate of cell viability decline. Baumann and colleagues exposed pancreatic cancer cells (PANC-1 and BxPC-3) to 45–50 °C for 5 min by means of a temperature-controlled bath, set to achieve and maintain target temperatures [72]. It was observed that subjecting cells to high temperatures (50 °C) can lead to nearly complete cell death after a single thermal exposure.

Moreover, our observations are in accordance with previous literature studies focused on the biological response of breast and pancreatic cancer cells undergoing NPs-mediated thermal treatments.

An investigation was conducted by Burke et al. to examine how human breast cancer stem cells and bulk breast cancer cells respond to heat treatment, specifically through water bath-mediated hyperthermia or multi-walled carbon nanotube-mediated thermal treatments [2]. The findings revealed that breast cancer stem cells show resistance to traditional hyperthermia at various temperature levels, and these heat treatments do not hinder the long-term ability of these cells to proliferate. Conversely, carbon nanotube-mediated thermal therapy resulted fatal for both stem and bulk breast cancer cells. The rapid necrosis that was attained as a result of nanotube-mediated thermal therapy sets it apart from the apoptotic cell death that is typically caused by classical hyperthermia [2].

Overall, in the present work, we evaluated the response of different cells to GNR-mediated PTT under the same treatment settings, to correlate a quantitative thermal analysis with cell viability and cell death pathways. Although the *in vivo* scenario is more complex and dependent on the host conditions, we strongly believe that understanding the cell response represents an important added value once operating in preclinical cancer models. This work also presents a relevant characterization of the temperature recording and monitoring component. It is important to underline that this aspect is not an end in itself, but it is extremely correlated with possible future exploitation at a preclinical and, above all, clinical level of this combined approach. Having intra-operative knowledge of the thermal phenomenon generated during stimulation is essential for the operator to understand some of the host's responses and possibly define future treatment lines.

The approach utilized in this study could be extended to other cell lines for the characterization of the thermotolerance and sensitivity upon NP-assisted PTT. Moreover, future investigations should be devised in *in vivo* conditions. Indeed, several *in vivo* studies have highlighted the potential of NP-assisted PTT for breast and pancreatic tumor treatment, mainly focusing on tumor regression, inhibition of tumor growth, and histological analyses [73]. Information on the spatial and temporal temperature evolution within the tumor region, as well as the performance of an accurate analysis based on different thermal parameters *in vivo* models, could help enlighten the correlation between the induced thermal effect with possible alteration of the tumor microenvironment upon NP-assisted photothermal exposures.

Author Statement

We the undersigned declare that this manuscript is original, has not been published before and is not currently being considered for publication elsewhere.

We confirm that the manuscript has been read and approved by all named authors and that there are no other persons who satisfied the criteria for authorship but are not listed.

We further confirm that the order of authors listed in the manuscript has been approved by all of us. We understand that the Corresponding Authors are the sole contacts for the Editorial process. They are responsible for communicating with the other authors about progress, submissions of revisions and final approval of proofs.

CRediT authorship contribution statement

Leonardo Bianchi: Writing – review & editing, Writing – original draft, Validation, Methodology, Investigation, Formal analysis, Data curation, Conceptualization. **Sara Baroni:** Writing – review & editing, Validation, Methodology, Investigation, Data curation. **Gabriela Paroni:** Writing – review & editing, Validation, Methodology, Investigation, Data curation. **Martina Bruna Violatto:** Writing – review & editing, Investigation. **Giulia Yuri Moscatiello:** Investigation. **Nicolò Panini:** Investigation. **Luca Russo:** Investigation. **Fabio Fiordaliso:** Writing – review & editing, Investigation. **Laura Colombo:** Investigation. **Luisa Diomede:** Writing – review & editing. **Paola Saccomandi:** Writing – review & editing, Supervision, Resources, Project administration, Funding acquisition. **Paolo Bigini:** Writing – review & editing, Supervision, Resources, Project administration.

Declaration of Competing Interest

The authors declare that they have no known competing financial interests or personal relationships that could have appeared to influence the work reported in this paper.

Data availability

Data will be made available on request.

Appendix A. Supplementary data

Supplementary data to this article can be found online at https://doi.org/10.1016/j.jphotobiol.2024.112993.

References

[1] H.S. Han, K.Y. Choi, Advances in nanomaterial-mediated Photothermal Cancer therapies: toward clinical applications, Biomedicines 9 (2021) 305.

[2] A.R. Burke, et al., The resistance of breast cancer stem cells to conventional hyperthermia and their sensitivity to nanoparticle-mediated photothermal therapy, Biomaterials 33 (2012) 2961–2970.

[3] R. Mooney, et al., Neural stem cell-mediated Intratumoral delivery of gold Nanorods improves Photothermal therapy, ACS Nano 8 (2014) 12450–12460.

[4] S.R. Dash, C.N. Kundu, Photothermal therapy: a new approach to eradicate Cancer, CNANO 18 (2022) 31–47.

[5] S. Korganbayev, A. Orrico, L. Bianchi, D. Paloschi, A. Wolf, A. Dostovalov, P. Saccomandi, PID controlling approach based on FBG Array measurements for laser ablation of pancreatic tissues IEEE trans. Instrum. Meas, IEEE Trans. Instrum. Meas. 1–9 (2021).

[6] L. Bianchi, S. Korganbayev, A. Orrico, M. De Landro, P. Saccomandi, Quasi-distributed fiber optic sensor-based control system for interstitial laser ablation of tissue: theoretical and experimental investigations, Biomed. Opt. Express 12 (2021) 2841.

[7] P. Lanka, et al., Estimation of porcine pancreas optical properties in the 600–1100 nm wavelength range for light-based therapies, Sci. Rep. 12 (2022) 14300.

[8] L. Sitia, et al., Combined ferritin Nanocarriers with ICG for effective phototherapy against breast Cancer, IJN 19 (2024) 4263–4278.

[9] L. Bianchi, et al., Fiber Bragg grating Sensors for thermometry during gold Nanorods-mediated Photothermal therapy in tumor model, in: *2020 IEEE SENSORS* 1–4 (IEEE, Rotterdam, Netherlands), 2020, https://doi.org/10.1109/SENSORS47125.2020.9278580.

[10] L. Bianchi, et al., Fiber Bragg grating Sensors-based thermometry of gold Nanorod-enhanced Photothermal therapy in tumor model, IEEE Sensors J. 22 (2022) 11297–11306.

[11] S.N. Turkmen Koc, S. Rezaei Benam, I.P. Aral, R. Shahbazi, K. Ulubayram, Gold nanoparticles-mediated photothermal and photodynamic therapies for cancer, Int. J. Pharm. 655 (2024) 124057.

[12] X. Huang, I.H. El-Sayed, W. Qian, M.A. El-Sayed, Cancer cell imaging and Photothermal therapy in the near-infrared region by using gold Nanorods, J. Am. Chem. Soc. 128 (2006) 2115–2120.

[13] S. Hwang, et al., Gold nanoparticle-mediated photothermal therapy: current status and future perspective, Nanomedicine 9 (2014) 2003–2022.

[14] A. Espinosa, et al., Cancer cell internalization of gold Nanostars impacts their Photothermal efficiency in vitro and in vivo: toward a Plasmonic thermal fingerprint in Tumoral environment, Adv. Healthc. Mater. 5 (2016) 1040–1048.

[15] J. Song, J. Qu, M.T. Swihart, P.N. Prasad, Near-IR responsive nanostructures for nanobiophotonics: emerging impacts on nanomedicine, Nanomedicine 12 (2016) 771–788.

[16] T. Yu, et al., Novel design of NIR-triggered plasmonic nanodots capped mesoporous silica nanoparticles loaded with natural capsaicin to inhibition of metastasis of human papillary thyroid carcinoma B-CPAP cells in thyroid cancer chemo-photothermal therapy, J. Photochem. Photobiol. B Biol. 197 (2019) 111534.

[17] E.B. Dickerson, et al., Gold nanorod assisted near-infrared plasmonic photothermal therapy (PPTT) of squamous cell carcinoma in mice, Cancer Lett. 269 (2008) 57–66.

[18] M. Zhang, H.S. Kim, T. Jin, W.K. Moon, Near-infrared photothermal therapy using EGFR-targeted gold nanoparticles increases autophagic cell death in breast cancer, J. Photochem. Photobiol. B Biol. 170 (2017) 58–64.

[19] L. Shao, et al., Light activation of gold nanorods but not gold nanospheres enhance antibacterial effect through photodynamic and photothermal mechanisms, J. Photochem. Photobiol. B Biol. 231 (2022) 112450.

[20] H. Norouzi, K. Khoshgard, F. Akbarzadeh, In vitro outlook of gold nanoparticles in photo-thermal therapy: a literature review, Lasers Med. Sci. 33 (2018) 917–926.

[21] H. Gamal, et al., A new vision of photothermal therapy assisted with gold nanorods for the treatment of mammary cancers in adult female rats, Nanoscale Adv. 6 (2024) 170–187.

[22] Z. Qin, J.C. Bischof, Thermophysical and biological responses of gold nanoparticle laser heating, Chem. Soc. Rev. 41 (2012) 1191–1217.

[23] P.K. Jain, K.S. Lee, I.H. El-Sayed, M.A. El-Sayed, Calculated absorption and scattering properties of gold nanoparticles of different size, shape, and composition: applications in biological imaging and biomedicine, J. Phys. Chem. B 110 (2006) 7238–7248.

[24] P. Saccomandi, E. Schena, S. Silvestri, Techniques for temperature monitoring during laser-induced thermotherapy: an overview, Int. J. Hyperth. 29 (2013) 609–619.

[25] P. Saccomandi, E. Schena, C.M. Pacella, New Horizons for Laser Ablation: Nanomedicine, Thermometry, and Hyperthermal Treatment Planning Tools, in: C.M. Pacella, T. Jiang, G. Mauri (Eds.), Image-guided Laser Ablation, Springer International Publishing, Cham, 2020, pp. 145–151, https://doi.org/10.1007/978-3-030-21748-8_15.

[26] V.P. Pattani, J.W. Tunnell, Nanoparticle-mediated photothermal therapy: a comparative study of heating for different particle types: nanoparticle-mediated photothermal therapy, Lasers Surg. Med. 44 (2012) 675–684.

[27] Y. Zhang, et al., Temperature-dependent cell death patterns induced by functionalized gold nanoparticle photothermal therapy in melanoma cells, Sci. Rep. 8 (2018) 8720.

[28] F. Chamani, et al., In vitro measurement and mathematical modeling of thermally-induced injury in pancreatic Cancer cells, Cancers 15 (2023) 655.

[29] L. Rahib, et al., Projecting Cancer incidence and deaths to 2030: the unexpected burden of thyroid, liver, and pancreas cancers in the United States, Cancer Res. 74 (2014) 2913–2921.

[30] U. Hani, et al., A systematic study of novel drug delivery mechanisms and treatment strategies for pancreatic cancer, J. Drug Deliv. Sci. Technol. 63 (2021) 102539.

[31] A. Lambert, T. Conroy, M. Ducreux, Future directions in drug development in pancreatic cancer, Semin. Oncol. 48 (2021) 47–56.

[32] R. Salvia, L. Addari, S. Paiella, Role of ablation Technologies in Locally Advanced Pancreatic Cancer, in: K. Søreide, S. Stättner (Eds.), Textbook of Pancreatic Cancer, Springer International Publishing, Cham, 2021, pp. 1267–1280, https://doi.org/10.1007/978-3-030-53786-9_82.

[33] H. Sung, et al., Global Cancer statistics 2020: GLOBOCAN estimates of incidence and mortality worldwide for 36 cancers in 185 countries, CA A Cancer J. Clin. 71 (2021) 209–249.

[34] T.H. Corbett, et al., Induction and chemotherapeutic response of two transplantable ductal adenocarcinomas of the pancreas in C57BL/6 mice, Cancer Res. 44 (1984) 717–726.

[35] R. Mooney, et al., Gold nanorod-mediated near-infrared laser ablation: in vivo experiments on mice and theoretical analysis at different settings, Int. J. Hyperth. 33 (2017) 150–159.

[36] Y. Niidome, et al., Surface modification of gold nanorods with synthetic cationic lipids, Chem. Commun. 3777 (2007), https://doi.org/10.1039/b706671f.

[37] K. Schnarr, et al., Gold nanoparticle-loaded neural stem cells for Photothermal ablation of Cancer, Adv. Healthc. Mater. 2 (2013) 976–982.

[38] C. Grabinski, et al., Effect of gold Nanorod surface chemistry on cellular response, ACS Nano 5 (2011) 2870–2879.

[39] E.J. Guggenheim, et al., Comparison of confocal and super-resolution reflectance imaging of metal oxide nanoparticles, PLoS One 11 (2016) e0159980.

[40] M.T. Silva, Secondary necrosis: the natural outcome of the complete apoptotic program, FEBS Lett. 584 (2010) 4491–4499.

[41] S. Lev, Targeted therapy and drug resistance in triple-negative breast cancer: the EGFR axis, Biochem. Soc. Trans. 48 (2020) 657–665.

[42] Zeng, et al., Chemoresistance in pancreatic cancer, IJMS 20 (2019) 4504.

[43] K.F. Chu, D.E. Dupuy, Thermal ablation of tumours: biological mechanisms and advances in therapy, Nat. Rev. Cancer 14 (2014) 199–208.

[44] V.P. Pattani, J. Shah, A. Atalis, A. Sharma, J.W. Tunnell, Role of apoptosis and necrosis in cell death induced by nanoparticle-mediated photothermal therapy, J. Nanopart. Res. 17 (2015) 20.

[45] S. Asadi, et al., Laser-induced optothermal response of gold nanoparticles: from a physical viewpoint to cancer treatment application, J. Biophotonics 14 (2021) e202000161.

[46] J. Domingo-Diez, et al., Effectiveness of gold Nanorods of different sizes in Photothermal therapy to eliminate melanoma and glioblastoma cells, IJMS 24 (2023) 13306.

[47] Á. Artiga, S. García-Embid, L. De Matteis, S.G. Mitchell, J.M. de la Fuente, Effective in vitro Photokilling by cell-adhesive gold Nanorods, Front. Chem. 6 (2018) 234.

[48] E. Happonen, et al., Thermal dose as a universal tool to evaluate nanoparticle-induced photothermal therapy, Int. J. Pharm. 587 (2020) 119657.

[49] S.A. Sapareto, W.C. Dewey, Thermal dose determination in cancer therapy, Int. J. Radiat. Oncol. *Biol. *Phys. 10 (1984) 787–800.

[50] G.C. van Rhoon, et al., CEM43°C thermal dose thresholds: a potential guide for magnetic resonance radiofrequency exposure levels? Eur. Radiol. 23 (2013) 2215–2227.

[51] P. Mertyna, W. Goldberg, W. Yang, S.N. Goldberg, Thermal ablation, Acad. Radiol. 16 (2009) 1539–1548.

[52] P.X.E. Mouratidis, I. Rivens, J. Civale, R. Symonds-Tayler, G. ter Haar, Relationship between thermal dose and cell death for "rapid" ablative and "slow" hyperthermic heating, Int. J. Hyperth. 36 (2019) 228–242.

[53] L. Roizin-Towle, J.P. Pirro, J. Mcdowell, A comparison of the heat and radiation sensitivity of rodent and human derived cells cultured in vitro, Int. J. Radiat. Oncol. *Biol. *Phys. 12 (1986) 647–653.

[54] G.M. Hahn, S.C. Ning, M. Elizaga, D.S. Kapp, R.L. Anderson, A comparison of thermal responses of human and rodent cells, Int. J. Radiat. Biol. 56 (1989) 817–825.

[55] S.C. Brüningk, et al., A comprehensive model for heat-induced radio-sensitisation, Int. J. Hyperth. 34 (2018) 392–402.

[56] B. Jang, Y.S. Kim, Y. Choi, Effects of gold Nanorod concentration on the depth-related temperature increase during Hyperthermic ablation, Small 7 (2011) 265–270.

[57] L. Bianchi, et al., Thermal analysis of laser irradiation-gold nanorod combinations at 808 nm, 940 nm, 975 nm and 1064 nm wavelengths in breast cancer model, Int. J. Hyperth. 38 (2021) 1099–1110.

[58] L. Talamini, et al., Influence of size and shape on the anatomical distribution of endotoxin-free gold nanoparticles, ACS Nano 11 (2017) 5519–5529.

[59] J. Fernandez Alarcon, et al., Long-term retention of gold nanoparticles in the liver is not affected by their physicochemical characteristics, Nanoscale 15 (2023) 8740–8753.

[60] Y. Ma, et al., The enhanced photo-thermal therapy of surface improved photoactive cadmium sulfide (CdS) quantum dots entrenched graphene oxide nanoflakes in tumor treatment, J. Photochem. Photobiol. B Biol. 192 (2019) 34–39.

[61] H. Chen, et al., Multifunctional gold Nanostar conjugates for tumor imaging and combined Photothermal and chemo-therapy, Theranostics 3 (2013) 633–649.

[62] B.D. Chithrani, A.A. Ghazani, W.C.W. Chan, Determining the size and shape dependence of gold nanoparticle uptake into mammalian cells, Nano Lett. 6 (2006) 662–668.

[63] C. Leduc, J.-M. Jung, R.R. Carney, F. Stellacci, B. Lounis, Direct investigation of intracellular presence of gold nanoparticles via Photothermal heterodyne imaging, ACS Nano 5 (2011) 2587–2592.

[64] G. Paroni, C. Brancolini, Measurement of caspase activity: from cell populations to individual cells, Methods Mol. Biol. 740 (2011) 65–79.

[65] R. Zheng, et al., Frontiers and future of immunotherapy for pancreatic cancer: from molecular mechanisms to clinical application, Front. Immunol. 15 (2024) 1383978.

[66] K.K. Bullock, A. Richmond, Beyond anti-PD-1/PD-L1: improving immune checkpoint inhibitor responses in triple-negative breast Cancer, Cancers 16 (2024) 2189.

[67] Kumar R. Vikas, S. Soni, Concentration-dependent photothermal conversion efficiency of gold nanoparticles under near-infrared laser and broadband irradiation, Beilstein J. Nanotechnol. 14 (2023) 205–217.

[68] M.T. Abo-Elfadl, et al., Photothermal therapeutic effect of PEGylated gold nano-semicubes in chemically-induced skin cancer in mice, J. Photochem. Photobiol. B Biol. 164 (2016) 21–29.

[69] E. Lacroce, et al., On the role of polymeric hydrogels in the thermal response of gold nanorods under NIR laser irradiation, Nanoscale Adv. 5 (2023) 6870–6879.

[70] J.K. Cheong, et al., Gold nanorods assisted photothermal therapy of bladder cancer in mice: a computational study on the effects of gold nanorods distribution at the Centre, periphery, and surface of bladder cancer, Comput. Methods Prog. Biomed. 230 (2023) 107363.

[71] T.H. Lee, et al., Sub-lethal hyperthermia promotes epithelial-to-mesenchymal-like transition of breast cancer cells: implication of the synergy between hyperthermia and chemotherapy, RSC Adv. 9 (2019) 52–57.

[72] K.W. Baumann, J.M. Baust, K.K. Snyder, J.G. Baust, R.G. Van Buskirk, Characterization of pancreatic Cancer cell thermal response to heat ablation or Cryoablation, Technol. Cancer Res. Treat. 16 (2017) 393–405.

[73] S.G. Alamdari, et al., Recent advances in nanoparticle-based photothermal therapy for breast cancer, J. Control. Release 349 (2022) 269–303.